A&A 503, 843–854 (2009)
DOI: 10.1051/0004-6361/200912060

Astronomy & Astrophysics

Analysis of the infrared spectra of the peculiar post-AGB stars EP Lyrae and HD 52961⋆

C. Gielen[1], H. Van Winckel[1], M. Matsuura[2,3], M. Min[4], P. Deroo[5,⋆⋆], L. B. F. M. Waters[1,4], and C. Dominik[4,6]

[1] Instituut voor Sterrenkunde, Katholieke Universiteit Leuven, Celestijnenlaan 200D, 3001 Leuven, Belgium
e-mail: clio.gielen@ster.kuleuven.be
[2] Astrophysics Group, Department of Physics and Astronomy, University College London, Gower Street, London WC1E 6BT, UK
[3] Division of Optical and IR Astronomy, National Astronomical Observatory of Japan, Osawa 2-21-1, Mitaka, Tokyo 181-8588, Japan
[4] Sterrenkundig Instituut "Anton Pannekoek", Universiteit Amsterdam, Kruislaan 403, 1098 Amsterdam, The Netherlands
[5] Jet Propulsion Laboratory, 4800 Oak Grove Drive, Pasadena, CA 91109, US
[6] Department of Astrophysics, Radboud University Nijmegen, PO Box 9010, 6500 GL Nijmegen, The Netherlands

Received 13 March 2009 / Accepted 9 June 2009

ABSTRACT

Aims. We aim to study in detail the peculiar mineralogy and structure of the circumstellar environment of two binary post-AGB stars, EP Lyr and HD 52961. Both stars were selected from a larger sample of evolved disc sources observed with Spitzer and show unique solid-state and gas features in their infrared spectra. Moreover, they show a very small infrared excess in comparison with the other sample stars.

Methods. The different dust and gas species are identified on the basis of high-resolution Spitzer-IRS spectra. We fit the full spectrum to constrain grain sizes and temperature distributions in the discs. This, combined with our broad-band spectral energy distribution and interferometric measurements, allows us to study the physical structure of the disc, using a self-consistent 2D radiative-transfer disc model.

Results. We find that both stars have strong emission features due to CO_2 gas, dominated by $^{12}C^{16}O_2$, but with clear $^{13}C^{16}O_2$ and even $^{16}O^{12}C^{18}O$ isotopic signatures. Crystalline silicates are apparent in both sources but proved very hard to model. EP Lyr also shows evidence of mixed chemistry, with emission features of the rare class-C PAHs. Whether these PAHs reside in the oxygen-rich disc or in a carbon-rich outflow is still unclear. With the strongly processed silicates, the mixed chemistry and the low $^{12}C/^{13}C$ ratio, EP Lyr resembles some silicate J-type stars, although the depleted photosphere makes nucleosynthetic signatures difficult to probe. We find that the disc environment of both sources is, to a first approximation, well modelled with a passive disc, but additional physics such as grain settling, radial dust distributions, and an outflow component must be included to explain the details of the observed spectral energy distributions in both stars.

Key words. stars: AGB and post-AGB – stars: binaries: general – stars: circumstellar matter – stars: individual: EP Lyrae – stars: individual: HD 52961

1. Introduction

The infrared spectra of post-AGB stars are often characterised by strong spectral signatures. These are formed in the gas and dust-rich circumstellar environment (CE), which is a remnant of the strong mass loss that occurred during the previous asymptotic giant branch (AGB) evolutionary phase. The chemistry in this circumstellar environment is found to be oxygen-rich or carbon-rich, depending on whether oxygen or carbon is more abundant. The less abundant of the two will be locked in the very stable CO molecule that forms in the stellar photosphere.

Typical post-AGB outflow sources that have O-rich CE not only show the well-known 9.7 and 18 μm features of amorphous silicates but also narrower features, arising from crystalline silicates (e.g. Waters et al. 1996; Molster et al. 2002). The condensates in C-rich outflows show features of carbon-species such as SiC, MgS or polycyclic aromatic hydrocarbons (PAHs) (e.g. Hony et al. 2001, 2002; Peeters et al. 2002). They are also characterised by an often very strong feature at 21 μm (Kwok et al. 1989; Volk et al. 1999; Hony et al. 2003). The photospheres of these 21 μm sources show strong enhancements of carbon and s-process elements (e.g. Reyniers et al. 2004, 2007) and the 21 μm stars are recognised as post-AGB carbon stars (e.g. Van Winckel & Reyniers 2000).

Some evolved objects show, however, features of both O-rich and C-rich dust species in their spectra. They are called mixed chemistry sources. This chemistry is detected in several sources in a wide range of different evolutionary stages. Some examples include Herbig Ae stars, or AGB stars, such as J-type carbon stars with silicate dust emission (Little-Marenin 1986; Lloyd Evans 1990). Others are red giants, for example HD 233517, an evolved O-rich red giant with PAHs in a circumstellar disc (Jura et al. 2006). Other examples are planetary nebulae (PNe) with evidence of silicates and PAHs (Kemper et al. 2002; Gutenkunst et al. 2008), or the hydrogen-poor [WC] central stars of PNe

⋆ Based on observations made with the 1.2 m Flemish Mercator telescope at Roque de los Muchachos, Spain, the 1.2 m Swiss Euler telescope at La Silla, Chile and on observations made with the Spitzer Space Telescope (program id 3274), which is operated by the Jet Propulsion Laboratory, California Institute of Technology under a contract with NASA.
⋆⋆ NASA Postdoctoral Fellow

Table 1. List of stellar parameters for our sample sources.

Name	α (J2000) (h m s)	δ (J2000) (° ′ ″)	$T_{\rm eff}$ (K)	$\log g$ (cgs)	[Fe/H]	$P_{\rm orb}$ (days)	e	$E(B-V)_{\rm tot}$	$L_{\rm IR}/L_*$ (%)	d (kpc)
EP Lyr	19 18 17.5	+27 50 38	7000	2.0	−1.5			0.51 ± 0.01	3 ± 0	3.2 ± 1.0
HD 52961	07 03 39.6	+10 46 13	6000	0.5	−4.8	1310	0.21	0.06 ± 0.02	12 ± 1	1.6 ± 0.5

Note: Listed are the name, equatorial coordinates α and δ(J2000), effective temperature $T_{\rm eff}$, surface gravity $\log g$, and metallicity [Fe/H] of our sample stars. For the model parameters we refer to De Ruyter et al. (2006). Also given are the orbital period and the eccentricity (see references in De Ruyter et al. 2006; Gielen et al. 2007). The total reddening $E(B-V)_{\rm tot}$, the energy ratio $L_{\rm IR}/L_*$ and the calculated distance, assuming a luminosity of $L_* = 3000 \pm 2000\,L_\odot$.

(Waters et al. 1998; Cohen et al. 1999). Also some M supergiants are associated with emission due to PAHs (Sylvester et al. 1998; Sloan et al. 2008).

Post-AGB stars with evidence of mixed chemistry include HD 44179, the central star of the carbon-rich Red Rectangle nebula (Cohen et al. 1975). The central star is a binary surrounded by a Keplerian O-rich circumbinary disc (e.g. Van Winckel et al. 1995; Waters et al. 1998; Men'shchikov et al. 2002; Bujarrabal et al. 2005). Here the formation of the disc is believed to have antedated the C-rich transition of the central star (e.g. Cohen et al. 2004; Witt et al. 2008).

Studies have shown that these evolved binaries with circumbinary discs are much more abundant than anticipated (De Ruyter et al. 2006; Van Winckel 2007). Interferometric studies (Deroo et al. 2006, 2007a) prove that the discs are indeed very compact, with radii around 50 AU in the N-band. The discs are also the natural environment of the observed photospheric chemical depletion pattern in these stars (Van Winckel et al. 1998; Giridhar et al. 2000), due to chemical fractionation by dust formation in the circumstellar environment (Waters et al. 1992) and subsequent accretion of the gas component. The presence of a long-lived stable reservoir of dust grains also could allow for the observed strong processing of the silicate dust grains, both in size as well as in crystallinity (Molster et al. 2002; Gielen et al. 2008).

Dusty RV Tauri stars are a distinct class in the post-AGB stars. They cross the instability strip, and are therefore pulsating stars (Jura 1986; Jura & Kahane 1999; De Ruyter et al. 2005). RV Tauri stars show large-amplitude photometric variations with alternating deep and shallow minima. The members are located in the high-luminosity end of the population II instability strip, and the photometric variations are interpreted as being due to radial pulsations. Circumstellar dust emission was observed in many of them (Jura 1986), and this was generally acknowledged to be a decisive character to place these stars in the post-AGB phase of evolution. The grains in almost all dusty RV Tauri stars are, however, not freely expanding but likely also trapped in a disc (Van Winckel et al. 1999; De Ruyter et al. 2005, 2006).

In this paper we focus on two peculiar post-AGB stars with RV Tauri pulsational characteristics: EP Lyr and HD 52961. These stars show unique spectral features and have very small infrared excesses in comparison to the larger sample.

The outline of the paper is as follows: We start with a short description of the programme stars in Sect. 2. In Sect. 3 we give an overview of the different observations and reduction strategies. The analysis based on the Spitzer spectra is given in Sect. 4 and subdivided in different subsections. Section 4.2 contains a description of the silicate dust features and the modelling of the Spitzer-IRS spectra. The CO_2 gas features are discussed in Sect. 4.3 and the observed PAH features in EP Lyr in Sect. 4.4. In Sect. 5 we model the observed SEDs using a passive disc model, also constrained with MIDI interferometric measurements. The discussion of our different results and our conclusions are presented in Sect. 6.

2. Programme stars

In our previous study we described and modelled the Spitzer-IRS spectra of 21 sources and found that the dust around these stars is all O-rich and on average highly crystalline (Gielen et al. 2008). The two stars discussed here have the lowest $L_{\rm IR}/L_*$, respectively 12% and 3%, in the larger Spitzer sample, where an average of about 50% was found. The large infrared luminosity can be explained with a passive disc model, provided that the inner rim is close to the star and the scale height of the disc is significant (e.g. Deroo et al. 2007a). The low observed $L_{\rm IR}/L_*$ values of both stars point to a small disc scale height and/or a much larger inner gap, as it is unlikely that a disc is optically thin in the radial direction. Not only do they have the lowest $L_{\rm IR}/L_*$ values, both stars show unique spectral signatures in comparison to the larger sample. We therefore selected these objects for a more detailed analysis.

2.1. EP Lyr

Schneller (1931) discovered the variability of EP Lyr and classified it as an RVb star. RVb stars are objects with a variable mean magnitude, in the General Catalogue of Variable Stars (Kholopov et al. 1999). Other studies (Zsoldos 1995; Gonzalez et al. 1997) classify the light curve as an RVa photometric variable, having a constant mean magnitude, with a period of $P = 83.46$ days. Preston et al. (1963) classify it as an RVB spectroscopic variable. Gonzalez et al. (1997) performed an abundance analysis on EP Lyr where they deduced stellar parameters (see Table 1) and found the star to be metal-poor, oxygen-rich and severely depleted. Using the molecular lines found in the spectra, they also quantified the $^{12}C/^{13}C$ ratio to be 9 ± 1. In the radial velocity data there is also evidence that EP Lyr must have a stellar mass companion, but additional observations are necessary to determine the orbit.

2.2. HD 52961

HD 52961 is an RV Tauri like object, similar to class RVb objects (Waelkens et al. 1991b), with a photometric variability of 72 days due to clear radial pulsations (Waelkens et al. 1991b). The binarity of HD 52961 was first reported by Van Winckel et al. (1995) and further refined in Van Winckel et al. (1999) and Deroo et al. (2006), where an orbital period of $P_{\rm orb} = 1297 \pm 7$ days and an eccentricity of $e = 0.22 \pm 0.05$ was found. On top of the stable photometric variation due to the pulsation, another long-term photometric variation was detected, correlated with the orbital period. Van Winckel et al. (1999) conclude that

this can be understood as caused by variable circumstellar extinction during the orbital motion.

The star is a highly metal-poor object with [Fe/H] = −4.8 (Waelkens et al. 1991a) and has an extremely high zinc to iron ratio of [Zn/Fe] = +3.1 (Van Winckel et al. 1992). The star is one of the most extremely depleted objects known.

HD 52961 has been studied with mid-IR long-baseline interferometry using the VLTI/MIDI instrument (Deroo et al. 2006). They find that the dust emission originates from a very small but resolved region, estimated to be ∼35 mas at 8 μm and ∼55 mas at 13 μm, likely trapped in a stable disc. The dust distribution through the disc is not homogeneous: the crystallinity is higher in the hotter inner region.

3. Observations

High- and low-resolution spectra of 21 post-AGB stars were obtained using the Infrared Spectrograph (IRS; Houck et al. 2004) aboard the Spitzer Space Telescope (Werner et al. 2004) in February 2005. The spectra were observed using combinations of the short-low (SL), short-high (SH) and long-high (LH) modules. SL (λ = 5.3–14.5 μm) spectra have a resolving power of $R = \lambda/\triangle\lambda \sim 100$, SH ($\lambda$ = 10.0–19.5 μm) and LH (λ = 19.3–37.0 μm) spectra have a resolving power of ∼600. Exposure times were chosen to achieve an S/N ratio of around 400 for the high-resolution modes, which we complemented with short exposures in low-resolution mode with an S/N ratio around 100, using the first generation of the exposure time calculator of the call for proposals.

The spectra were extracted from the SSC data pipeline version S13.2.0 products, using the c2d Interactive Analysis reduction software package (Kessler-Silacci et al. 2006; Lahuis et al. 2006). This data processing includes bad-pixel correction, extraction, defringing and order matching. To match the different orders, we applied small scaling corrections.

4. Spectral analysis

4.1. General

A look at the spectra of EP Lyr and HD 52961 (Fig. 1) show very rich spectra with quite different continuum slopes. EP Lyr shows strong emission features at longer wavelengths, with peak emission in the 20 μm region, whereas HD 52961 is characterised by a strong 10 μm emission feature on top of a much steeper continuum.

Common dust species found in oxygen-rich post-AGB stars are amorphous silicates, namely olivine and pyroxene. Amorphous olivine ($Mg_{2x}Fe_{2(1-x)}SiO_4$, where $0 \leq x \leq 1$ denotes the magnesium content) has very prominent broad features around 9.8 μm and 18 μm. Amorphous pyroxene ($Mg_xFe_{1-x}SiO_3$) shows a 10 μm feature similar to that of amorphous olivine, but shifted towards shorter wavelengths. Also the shape of the 18 μm feature is slightly different. For EP Lyr it is unclear whether there is a significant contribution of amorphous silicates. Small amorphous silicates could contribute to the observed strong emission bump at 20 μm in EP Lyr, but as there does not seem to be a 10 μm amorphous feature, the 20 μm bump could be purely continuum dominated. HD 52961 has clear strong emission of amorphous silicates at 10 μm, but the profile shows complex narrow subfeatures. Very little contribution at 20 μm is seen.

Both stars show strong narrow emission features which can be identified as being due to crystalline silicates.

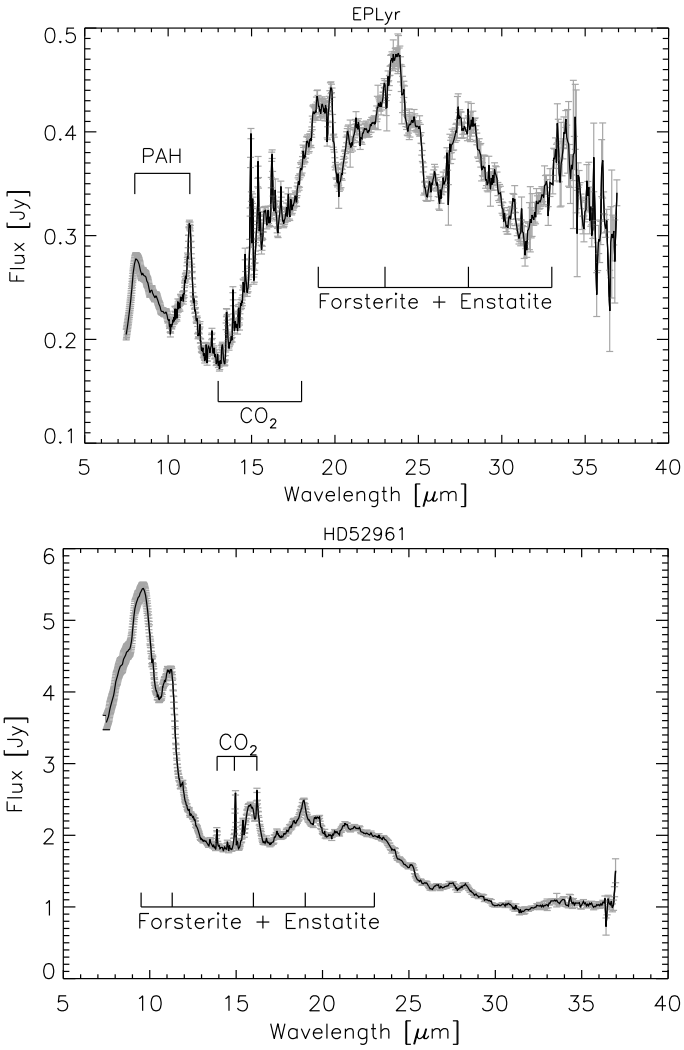

Fig. 1. The combined Spitzer-IRS high- and low-resolution spectrum of EP Lyr (*top*) and HD 52961 (*bottom*). In grey we overplot the estimated errors.

The Mg-rich end members of crystalline olivine and pyroxene, forsterite (Mg_2SiO_4) and enstatite ($MgSiO_3$), show strong but narrow features at distinct wavelengths around 11.3 – 16.2 – 19.7 – 23.7 – 28 and 33.6 μm. For EP Lyr the silicate emission only clearly starts longward of 18 μm, where strong emission features around 19 – 23 – 27 and 33 μm can be seen. HD 52961 has strong narrow features at 9.8 – 11.3 μm and a remarkably strong 16 μm feature. If this strong 16 μm band is only due to forsterite it has shifted considerably to shorter wavelengths. A significant 16 μm feature is seen in several evolved disc sources but it is never as strong as in HD 52961 (Gielen et al. 2008).

EP Lyr shows evidence of the presence of carbon-rich dust species with probable PAH identifications at 8.1 and 11.3 μm. The detection of PAH emission together with silicates is surprising and only observed in a few other post-AGB sources. The analysis of the PAH features is given in Sect. 4.4.

The spectrum of EP Lyr shows a strong resemblance to that of IRAS 09245-6040 (Fig. 3), a silicate J-type carbon AGB star (Molster et al. 2001; García-Hernández et al. 2006). Silicate J-type carbon stars have surprisingly low $^{12}C/^{13}C$ ratios and do not show the typical s-process overabundances seen in N-type carbon stars (Abia & Isern 2000). The infrared spectrum of

these stars shows features of both carbon- and oxygen-rich dust species.

Of the silicate J-type carbon stars, only 10% show emission bands due to crystalline material (Lloyd Evans 1991; Ohnaka & Tsuji 1999). The formation history of these stars is still unclear, but the most promising scenario for the presence of silicates in these stars, is that they are binaries with an undetected companion (Lloyd Evans 1990; Yamamura et al. 2000). A disc is supposed to be formed when the primary was still an O-rich giant. After that the star underwent thermal pulses and evolved into a carbon star. The silicate disc could be either captured from the wind (Mastrodemos & Morris 1999) or the result of a phase of strong binary interaction in a narrow system. Systems with strong crystalline features in their spectra, such as IRAS 09425-6040 or IRAS 18006-3213 (Deroo et al. 2007b), would then be a result of mass-transfer into a circumbinary system, whereas sources dominated by amorphous silicates, such as V778 Cygni (Yamamura et al. 2000) or BH Gem (Ohnaka et al. 2008), consist of a wide binary with a circumcompanion disc. To date, no orbits are known, however, and direct evidence of binarity is found in a few objects only (Izumiura et al. 2008).

For IRAS 09245-6040, the $^{12}C/^{13}C$ ratio is calculated to be 15 ± 6 (García-Hernández et al. 2006). In the ISO-SWS spectrum features of C_2H_2, HCN, CO, C_3 and SiC are seen shortward of 15 μm; after 15 μm the spectrum is dominated by strong emission features of Mg-rich crystalline silicates (Molster et al. 2001). As in EP Lyr, there is no evidence of a strong contribution of amorphous silicates.

Finally in both EP Lyr and HD 52961, clear CO_2 gas emission features are detected the 13–18 μm region. This is discussed in Sect. 4.3.

4.2. Silicate dust emission

We optimised the fitting procedure as discussed in Gielen et al. (2008) for these two outliers, where we modelled the full Spitzer sample, consisting of 21 stars. In short we assume the flux to be originating from an optically thin region, so we can make linear combinations of the absorption profiles to calculate the model spectrum. In our previous modelling we found that, on average for the full sample, the best fit was obtained using relatively large grains ($\geq$2 μm) in an irregular Gaussian Random Fields (GRF) dust model. For EP Lyr and HD 52961 however, we already found that using smaller grain sizes ($\leq$2 μm) improved the fit considerably.

So we repeated the analysis for EP Lyr and HD 52961, allowing for different dust shapes, grain sizes and Mg/Fe content in the amorphous grains. We tested Mie, GRF and DHS (Distribution of Hollow Spheres) dust models in grain sizes ranging from 0.1 to 4.0 μm. In order to test for the presence of Fe-poor amorphous dust, we perform the modelling both with pure Mg-rich amorphous silicates ($x = 1$) and with the more standard Mg-Fe amorphous silicate dust ($x = 0.5$). For a detailed description of the fitting routine we refer to Gielen et al. (2008). The results of the fitting can be found in Table 2. As for EP Lyr the silicate signatures only appear after 18 μm; we only fit this part of the Spitzer spectrum.

The χ^2 values of our fitting (Table 2) are still quite high for HD 52961 but, confirming the result of Gielen et al. (2008), we can already tell that for both stars Mie theory is not a good dust approximation. For EP Lyr the GRF grains prove the best match, but the difference in χ^2 with the small DHS grain approximation is only minimal. The best fit to EP Lyr is obtained using both small (0.1 μm) and larger (2.0 μm) silicate grains. The small difference in calculated χ^2 values for EP Lyr is due to the low signal-to-noise ratio, making it hard to distinguish between different synthetic emission profiles. For HD 52961 small grains in Mg-rich silicates give the best χ^2. Plots of our best fitting models can be found in Fig. 2. Table 3 gives the resulting parameters.

Table 2. χ^2 values for different models used in our full spectral fitting.

	EP Lyr χ^2	HD 52961 χ^2	model description
model1	21.7	129.4	Mie - 0.1–2.0 μm - $x = 0.5$
model2	6.2	67.5	DHS - 0.1–1.5 μm - $x = 0.5$
model3	6.2	63.8	DHS - 0.1–1.5 μm - $x = 1.0$
model4	8.4	101.4	DHS - 1.5–3.0 μm - $x = 0.5$
model5	8.6	140.8	DHS - 1.5–3.0 μm - $x = 1.0$
model6	5.9	64.2	GRF - 0.1–2.0 μm - $x = 0.5$
model7	6.3	50.0	GRF - 0.1–2.0 μm - $x = 1.0$
model8	5.8	96.5	GRF - 2.0–4.0 μm - $x = 0.5$
model9	5.4	72.2	GRF - 2.0–4.0 μm - $x = 1.0$

Note: For each model we give the used dust approximation, grain size and Mg-Fe content in the amorphous grains. $x = 1.0$ denotes pure Mg-rich amorphous dust, $x = 0.5$ the more standard Mg-Fe amorphous silicates.

The large χ^2 value of HD 52961 quantifies that this star has a very peculiar, unique chemistry, and we did not succeed in explaining all of the observed features. The strong forsterite 11.3 μm feature in the GRF dust approximation is clearly too broad. DHS grains fit the feature better, but other feature profiles are fitted less well with this approximation. There also appears to be a short wavelength shoulder on the amorphous 9.8 μm feature, which is not explained in the modelling. The strong 16.5 μm feature is not reproduced in central wavelength by any of the different models. We already observed this trend in our full sample fitting (Gielen et al. 2008), where the feature seemed to be shifted bluewards in comparison with the mean spectrum of the full sample. The two narrow features around 19 μm could be an artifact of the data reduction, since in this region there can be a bad overlap between the SH and LH Spitzer-IRS high-resolution bands.

For EP Lyr we fit the spectrum longwards of 18 μm, where the silicate features are seen. This gives dust temperatures between 100 and 230 K. This model, however, does not fit the spectrum before 18 μm, since the continuum does not follow the observed strong downward slope before 20 μm. If we try to fit the full Spitzer wavelength range we find we can get a better fit to the underlying continuum but then the features at 27 and 33 μm are much stronger in the observed spectrum than in our best model. Unlike in other sources, a two temperature approach fails to model both the observed continuum and the coolest features for the full Spitzer wavelength spectrum of EP Lyr. Irrespective of the derived continuum temperature, all the tested models give estimates of the dust temperatures between 100–300 K, which agrees with the temperatures derived in the SED modelling (Sect. 5). Clearly, the crystalline dust particles must be quite cold.

4.3. CO_2 emission

4.3.1. Introduction

CO_2 emission has been found in approximately 30% of all O-rich AGB stars (Justtanont et al. 1998; Ryde et al. 1999; Sloan et al. 2003), but CO_2 detections in post-AGB stars are rare. To our knowledge CO_2 gas has been found in only two

Table 3. Listed are the best fit parameters deduced from our full spectral fitting.

Name	χ^2	$T_{\rm dust1}$ (K)	$T_{\rm dust2}$ (K)	Fraction $T_{\rm dust1}$–$T_{\rm dust2}$	$T_{\rm cont1}$ (K)	$T_{\rm cont2}$ (K)	Fraction $T_{\rm cont1}$–$T_{\rm cont2}$
EP Lyr	5.4	114^{122}_{14}	228^{488}_{89}	$0.9^{0.1}_{0.6} - 0.1^{0.6}_{0.1}$	205^{702}_{103}	641^{331}_{301}	$0.96^{0.02}_{0.06} - 0.04^{0.06}_{0.02}$
HD 52961	50.0	200^{10}_{0}	724^{186}_{96}	$0.9^{0.0}_{0.1} - 0.1^{0.1}_{0.0}$	111^{356}_{11}	996^{4}_{111}	$0.99^{0.00}_{0.03} - 0.01^{0.03}_{0.00}$

Name	Olivine Small - Large	Pyroxene Small - Large	Forsterite Small - Large	Enstatite Small - Large	Continuum
EP Lyr	6^{41}_{6}–5^{25}_{5}	8^{34}_{7}–6^{23}_{6}	34^{19}_{15}–9^{33}_{8}	5^{20}_{5}–28^{17}_{21}	53^{11}_{20}
HD 52961	0^{13}_{0}–1^{41}_{1}	55^{12}_{18}–2^{43}_{2}	6^{18}_{5}–33^{13}_{18}	1^{8}_{1}–3^{26}_{3}	69^{4}_{4}

Note: Top part: The χ^2, dust and continuum temperatures and their relative fractions. Bottom part: The abundances of small (0.1 μm) and large (2.0 μm) grains of the various dust species are given as fractions of the total mass, excluding the dust responsible for the continuum emission. The last column gives the continuum flux contribution, listed as a percentage of the total integrated flux over the full wavelength range. The errors were obtained using a Monte-Carlo simulation based on 100 equivalent spectra. Details of the modelling method are explained in Gielen et al. (2008).

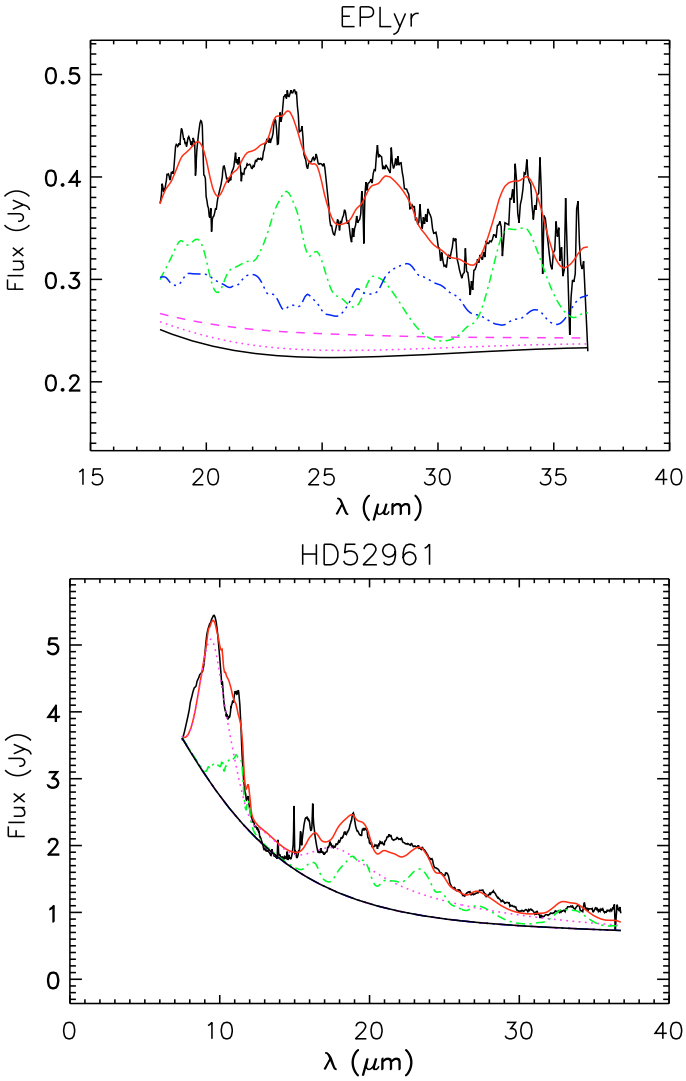

Fig. 2. Best fits for EP Lyr and HD 52961. The observed spectrum (black curve) is plotted together with the best model fit (red curve) and the continuum (black solid line). Forsterite is plotted in dash-dot lines (green) and enstatite in dash-dot-dotted lines (blue). Small amorphous grains are plotted as dotted lines (magenta) and large amorphous grains as dashed lines (magenta).

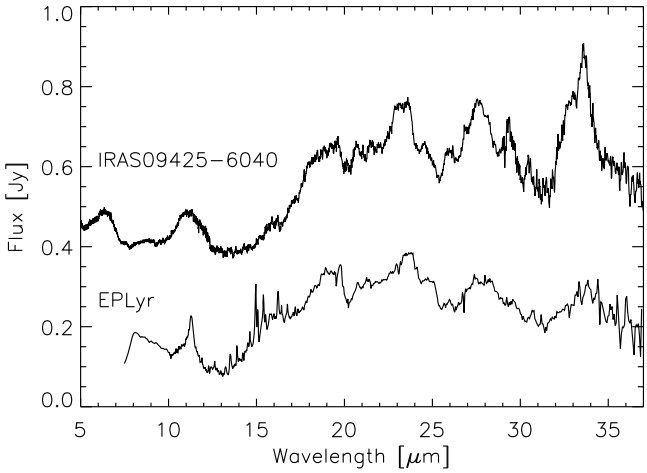

Fig. 3. The Spitzer-IRS spectrum of EP Lyr compared to the ISO-SWS spectrum of IRAS 09425-6040. The spectrum of IRAS 09425-6040 is normalised and offset for comparison.

post-AGB stars, the Red Rectangle and HR 4049 (Waters et al. 1998; Cami & Yamamura 2001), which are also binaries surrounded by a stable circumstellar disc. HR 4049 is the only example of a post-AGB star showing CO_2 in emission in the 13–16 μm region. Cami & Yamamura (2001) argued that the isotopic distribution of oxygen in HR 4049 is abnormal, based on the isotope ratio analysis of the CO_2 emission features. This was not confirmed by Hinkle et al. (2007), who use high-resolution spectra of the fundamental and first overtone CO vibro-rotational transition in the near-IR.

Both EP Lyr and HD 52961 show clear gas phase emission lines of $^{12}CO_2$ and $^{13}CO_2$. These emission lines were also seen in only one other source in our Spitzer sample (Gielen et al. 2008), namely in IRAS 10174-5704.

The CO_2 emission of EP Lyr seems to be lying on top of a "plateau" that extends from 13 to 17 μm. A similar plateau in this region is observed in PAH-rich sources (Peeters et al. 2004), but this plateau is much broader and ranges from 15 to 20 μm and is often characterised by strong emission features at 16.4 μm (and less prominent at 15.8, 17.4 and 19 μm), and thus quite different to the one seen in EP Lyr.

4.3.2. Analysis

To retrieve the very rich spectral information of the CO_2 emission bands, we calculate spectra of CO_2, using HITRAN line lists (Rothman et al. 2005) and a circular slab model for the radiative-transfer (Matsuura et al. 2002). The model has four parameters: the excitation temperature ($T_{\rm ex}$), the total CO_2 column

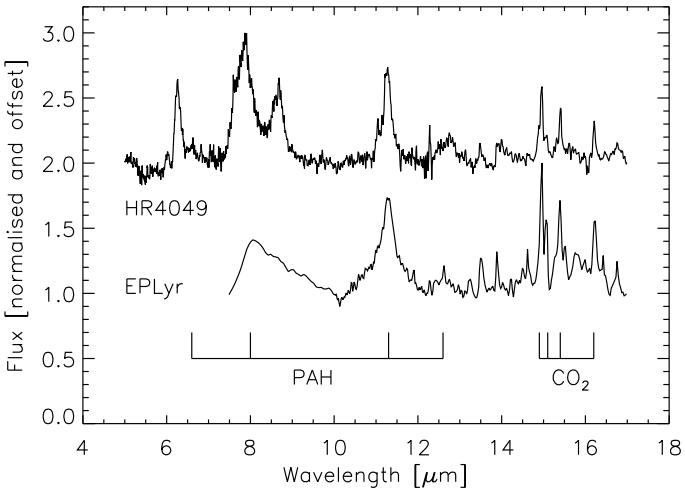

Fig. 4. Comparison between the continuum-subtracted spectrum of EP Lyr and HR 4049, another mixed chemistry source. Both stars show clear emission due to CO_2 gas around 15 μm and strong PAH features before 13 μm. The CO_2 features at 14.9–16.2 μm, 15.3 μm and 15.1 μm are respectively due to $^{12}C^{16}O_2$, $^{13}C^{16}O_2$ and $^{16}O^{12}C^{18}O$. The PAH emission is clearly very different in HR 4049, where class B PAHs are found, whereas in EP Lyr the PAH features can be attributed to class C (see Sect. 4.4).

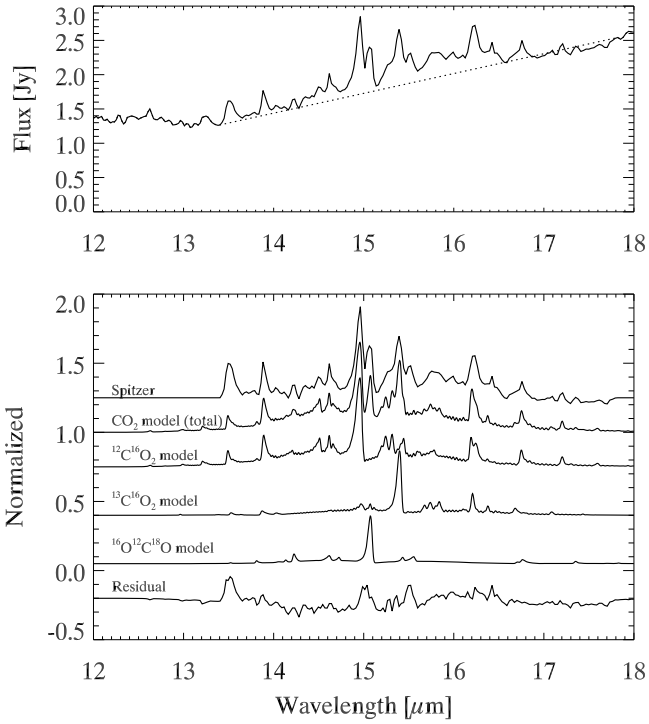

Fig. 5. EP Lyr: top panel shows the observed spectrum (solid line) and pseudo-continuum spectra (dotted line). The bottom panel shows the continuum divided spectrum, CO_2 model spectra (combining all of the isotopes) and individual CO_2 isotope spectra (from top to bottom $^{12}C^{16}O_2$, $^{13}C^{16}O_2$, $^{16}O^{12}C^{18}O$).

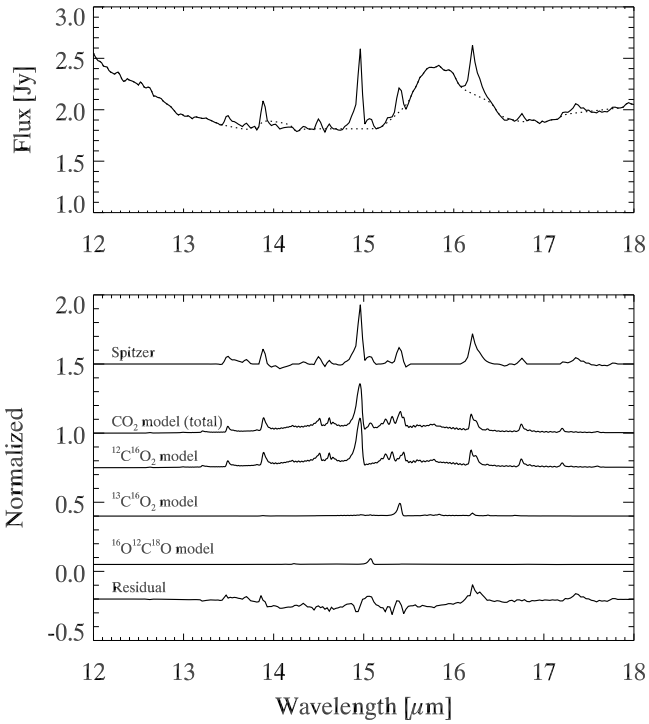

Fig. 6. Same as Fig. 5 but for HD 52961.

density (N), the radius of CO_2 gas (r) and the isotope ratio. The radius of the CO_2 layer is given relative to the radius of the background continuum source at 13 μm. The dependence of the CO_2 model spectra on these parameters are described by Cami & Yamamura (2001). We estimate a pseudo-continuum by using a spline fit and a linear fit for HD 52961 and EP Lyr, respectively. For HD 52961, we interpolate the spectrum at the spectral range where CO_2 bands have little influence on the observed spectrum. The continuum was also chosen so that the forsterite feature at 16 μm would be removed. A spline fit was tested for EP Lyr but failed because of the richness of CO_2 features in the mid-infrared range, so we simply use a linear interpolation between 13.4 and 17.8 μm. Estimated continua are displayed as dotted lines in the top panels of Figs. 5 and 6. The resulted parameters for the model calculations are summarised in Table 4, and the resulted spectra show the identifications of the different CO_2 bands (bottom panels of Figs. 5 and 6).

Many small features in EP Lyr in the 13.5–17 μm region are due to CO_2: features at 13.5, 13.9, 14.7, 14.9, 16.2 μm are attributed to the CO_2 main isotope $^{12}C^{16}O_2$. The main isotopic $^{12}C^{16}O_2$ bands are probably optically thick, surpressing the line intensities. $^{13}C^{16}O_2$ and $^{16}O^{12}C^{18}O$ bands are found at 15.3 μm and 15.1 μm, respectively. The prominent $^{16}O^{12}C^{18}O$ feature is surprising. This feature was also found in the other binary post-AGB star HR 4049 (Cami & Yamamura 2001).

The model uses a high fraction of isotopes, but actual abundance ratios remain largely uncertain, mainly because of the uncertainty of the interpolated continuum spectrum and the optical thickness of the main isotope. Nevertheless, these two features are particularly prominent in the spectrum of EP Lyr, more than in HD 52961, suggesting different isotope ratios for EP Lyr. We see that the observed "plateau" in EP Lyr can be explained by the richness of the $^{12}C^{16}O_2$ features, but the $^{12}C/^{13}C$ ratio is confirmed to be low. The strength of the isotopes, including the very rare ^{18}O (in the Sun $^{16}O/^{18}O$ is ~500), is an exclusive feature of post-AGB stars.

4.4. PAH features

Polycyclic aromatic hydrocarbons are found in a large variety of objects, including the diffuse ISM, HII regions, young stellar objects, post-AGB stars and planetary nebulae. They have strong emission features in the 3–13 μm region (e.g. Tielens 2008).

Table 4. Resulting parameters for the model calculations. The isotope ratio is as follows: $^{12}C^{16}O_2$:$^{13}C^{16}O_2$:$^{16}O^{12}C^{18}O$.

	T_{ex} (K)	N (cm^{-2})	r (R_*)	isotope ratio
EP Lyr	900	8×10^{18}	4.7	0.7 : 0.2 : 0.1
HD 52961	800	5×10^{18}	4.7	0.93 : 0.05 : 0.02

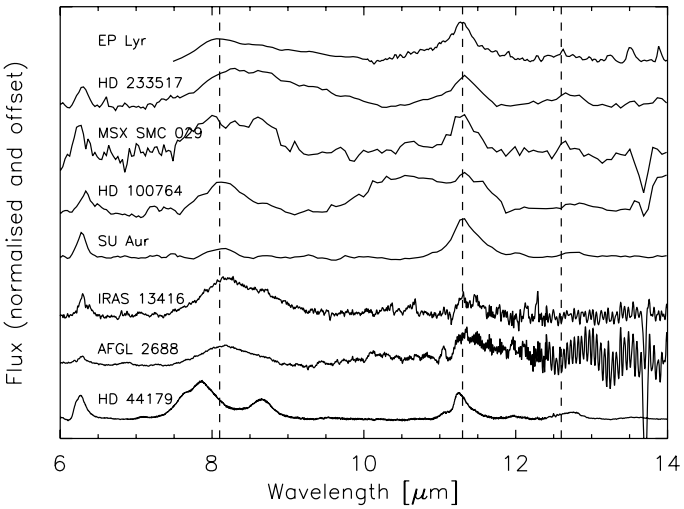

Fig. 7. Continuum-subtracted spectra (based on a spline fit) of class-C sources as described in Sloan et al. (2007). The vertical dashed lines are at 8.1, 11.3 and 12.6 μm. For comparison we also plot HD 44179, which has class B PAH emission.

The feature at 3.3 μm arises from the C-H stretching mode of neutral PAHs. The C-C modes produce features with typical central wavelengths at 6.2 and 7.7 μm. The 8.6 μm feature is due to C-H in-plane bending modes and features longward of 10 μm can be attributed to C-H out-of-plane bending modes.

Peeters et al. (2002) defined three groups of PAH spectra based on their emission profiles and peak positions. The "class A" sources have features at 6.22, 7.6 and 8.6 μm. "Class B" sources show the same features but shifted to the red, peaking at 6.27, 7.8 and >8.6 μm. They also identified two "class C" sources, the Egg Nebula (AFGL 2688) and IRAS 13416-6243, both post-AGB objects. These rare "class C" sources show emission features at 6.3 μm, no emission near 7.6 μm, and a broad feature centred around 8.2 μm, extending beyond 9 μm.

With the release of the IRS aboard the Spitzer Space Telescope, a limited number of additional class-C sources were discovered (Fig. 7). MSX SMC 029, a class-C post-AGB star in the SMC, was detected by Kraemer et al. (2006). Sloan et al. (2007) report on the detection of class-C PAH features in HD 100764, a carbon-rich red giant with evidence of a circumstellar disc. Jura et al. (2006) also report on the detection of class-C PAH features in a circumstellar disc around the oxygen-rich K-giant HD 233517. Two young objects, the T Tauri star SU Aur (Furlan et al. 2006) and the Herbig Ae/Be source HD 135344 (Sloan et al. 2005), also show PAH spectra of class C, although in HD 135344 the PAH features seem to be somewhat more in between B and C. This source is also slightly hotter than other class C sources. A comparison of the PAH features in all these sources is given by Sloan et al. (2007). They find that all the known class-C spectra are excited by relatively cool stars of spectral type F or later and argue that the hydrocarbons in these sources have not been exposed to much ultraviolet radiation. The class-C PAHs are then relatively protected and unprocessed, while class A and B PAHs have been exposed to more energetic photons and are hence more processed.

EP Lyr shows PAH emission bands at 8.1, 11.3 and 12.6 μm. Other features can be seen at 13.25 μm. Whether these can be attributed to PAHs remains uncertain. The PAH spectrum of EP Lyr can be classified as class C. EP Lyr is a high amplitude-variable with an effective temperature around 7000 K, which is on the hot end of the other class-C emitters (see Sloan et al. 2007).

Sofar, it is not clear whether the PAH carriers reside in the circumbinary disc, or in bipolar lobes created by a more recent mass-loss event, as observed in HR 4049 (Johnson et al. 1999; Dominik et al. 2003; Antoniucci et al. 2005; Hinkle et al. 2007; Menut et al. 2009) and in the Red Rectangle (Men'shchikov et al. 2002; Cohen et al. 2004). For HR 4049, Johnson et al. (1999) found that the optical polarisation seems to vary with orbital phase, suggesting that the polarisation in the optical is due to scattering in the circumbinary disc. In the UV, the polarisation is caused by scattering in the bipolar lobes, which should contain a population of small grains, including the PAH carriers. HR 4049 and HD 44179, as well as EP Lyr and HD 52961, are strongly depleted, and molecules or the formation of dust in these very depleted environments is likely very different from solar condenstation. As the CO molecule is abundant in the circumstellar environment, accretion of circumstellar gas will likely result in a C~O photosphere. HR 4049 and HD 44179 are stars with PAH emission belonging to the more standard class B.

Unlike what is detected around HD 44179 (the ERE nebula) and HR 4049 (nano-diamonds), for EP Lyr the PAHs are the only carbon-rich component observed in the circumstellar spectra. There is no evidence that the photosphere of EP Lyr is in, or went through, a carbon-rich phase. The photosphere is depleted so that nucleosynthetic yields are very hard to recognise, but the photosphere is clearly oxygen-rich (Gonzalez et al. 1997). A scenario involving hot-bottom burning to return to an oxygen-rich condition after a carbon-rich phase in the stellar evolution along the AGB is very unlikely: it would imply the object is of a more massive origin (Lattanzio et al. 1996; McSaveney et al. 2007), which is in contradiction with its Galactic coordinates of $b = 6.9°$. Assuming 10 000 $L_\odot$ for a putative massive progenitor, the distance above the Galactic plane would be about 660 pc, which is very high for an object of 5–6 $M_\odot$. Moreover, the initial metallicity is likely subsolar as indicated by the sulfur and zinc abundances. Although, with the depletion, it is unclear whether these abunances of the volatiles do indeed represent the initial conditions. Also the pulsation period of EP Lyr is similar to other RV Tauri objects which are of low initial mass. We conclude that the photosphere of EP Lyr is now O-rich, and we argue it is very unlikely that it was ever in its history in a carbon-rich phase. The PAH synthesis likely occurred in O-rich conditions.

As Fig. 8 shows, the spectrum of EP Lyr has a striking resemblance to that of HD 233517, shortward of 13 μm (Jura et al. 2006). Jura (2003) hypothesises that HD 233517 was a short-period binary on the main sequence. A circumstellar disc was then formed when the companion star was engulfed by the more massive star when it entered giant evolution, followed by a phase of strong mass ejection in the equatorial plane. Since HD 233517 is an oxygen-rich star, it is remarkable that the disc shows features of carbon-rich chemistry. Jura et al. (2006) propose a scenario in which the PAHs could be formed inside the disc due to Fischer-Tropsch (FT) catalysis on the surface of solid iron grains. These FT reactions can convert CO and H_2 into water and hydrocarbons (Willacy 2004), these hydrocarbons could then be converted in into PAHs.

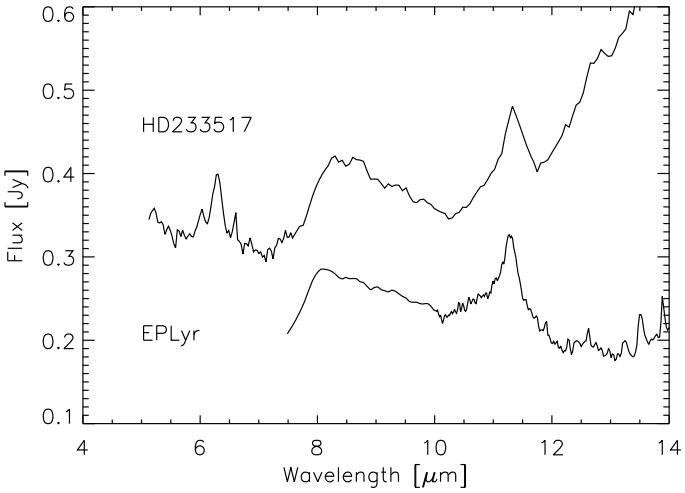

Fig. 8. Comparison between the Spitzer-IRS spectrum of HD 233517 and EP Lyr in the 6–14 μm region.

So far it remains unclear whether the shape of the observed emission features can detect if the PAH carriers reside in the disc or an outflow.

5. Spectral energy distribution

5.1. 2D disc modelling

For both stars extensive photometric data are available. This, together with the Spitzer infrared spectral information, allows us to constrain some of the physical characteristics of the circumbinary disc.

We fit the SED using a Monte Carlo code, assuming 2D-radiative-transfer in a passive disc model (Dullemond et al. 2001; Dullemond & Dominik 2004). This code computes the temperature structure and density of the disc. The vertical scale height of the disc is computed by an iteration process, demanding vertical hydrostatic equilibrium. The distribution of dust grain properties is fully homogeneous and, although this model can reproduce the SED, dust settling timescales indicate that settling of large grains to the midplane occurs. Using the dust settling timescale

$$t_{\rm set} = \frac{\pi}{2}\frac{\Sigma_0}{\rho_d a}\frac{1}{\Omega_k}\ln\frac{z}{z_0}$$

with Σ_0 the surface density, ρ_d the particle density, a the grain size and $\Omega_k = \sqrt{\frac{GM_*}{r^3}}$ the Keplerian rotation rate (Miyake & Nakagawa 1995), we find that grains with sizes between 500 μm and 0.1 cm can descend 50 AU on timescales similar to the estimated lifetime of the disc. An inhomogeneous disc model with a vertical gradient in grain-size distribution is thus necessary (Gielen et al. 2007). These large and cooler grains in the disc midplane mainly contribute to the far-IR part of the SED and constitute the main fraction of the total dust mass. The disc structure and near- and mid-IR flux are almost fully determined by small grains. So we use a homogeneous 2D disc model to fit the near- and mid-IR part of the SED and add a single blackbody temperature to represent the cooler midplane made up of large grains. The lack of observational constraints on the temperature structure of this component does not allow us to constrain this extra parameter.

Stellar input parameters of the model are the luminosity, the total mass (we assume the total gravitational potential to be spherically symmetric with a total mass of $M = 1\,M_\odot$), and $T_{\rm eff}$. The luminosity (and thus the distance) for these sources is not well constrained so we use values between $L = 1000$–$5000\,L_\odot$, typical values for post-AGB sources. Input disc parameters are $R_{\rm in}$ and $R_{\rm out}$, the different dust components, the total disc mass and the power law for the surface-density distribution. Since we are not dealing with outflow sources a power law $\alpha > -2$ is used. The gas-to-dust ratio is kept fixed at 100.

The modelling is still degenerate, especially in parameters like the outer radius and the total disc mass which can be easily interchanged, without strongly influencing the SED. We use a dust mixture of amorphous and crystalline silicates in grain sizes ranging of 0.1–20 μm, with a power law distribution of −3.0, for the homogeneous disc. For HD 52961 the 850 μm submillimetre data points to the presence of extremely large grains in the disc, but these large grains are assumed not to influence the near- and mid-IR part of the SED, and will only be important for the blackbody component. We use a value of 300 AU for $R_{\rm out}$. For the inner rim we use the radius at which the temperature of the inner rim equals about 1500 K. This is a typical value for the dust sublimation temperature of silicates, although values as low as 1200 K are sometimes also used. The total SED energetics are then calculated, given a specific inclination angle of the system.

We do not aim to reproduce the observed narrow features in the Spitzer spectrum, since these features originate from an optically thin upper layer of small grains at the disc surface. They can only be fitted well using an inhomogeneous disc model with grain settling. Instead, we want to model the observed general energetics of the SED spectrum, thus the observed continuum and amorphous dust features.

5.2. Comparison with interferometric data

The circumstellar environment of HD 52961 has been resolved using the VLTI/MIDI instrument, with angular sizes in the N-band between 35 mas and 55 mas in a uniform disc approximation (Deroo et al. 2006). EP Lyr is too faint for current interferometric capabilities.

To compare our disc model of HD 52961 with the MIDI data we made model images from which we extracted visibilities, using the same projected baseline lengths (40 m/46 m) and angles (45°/46°) as the observations. The only free parameters here are the inclination of the disc and the orientation angle of the system on the sky. A range of inclinations which still fit the observed SED was tested, in steps of 15°. The orientation angle is varied 1° at a time. The result of this comparison can be found in Sect. 5.3.1.

5.3. Results

When modelling the near- and mid-IR part of the SEDs, the feature-to-continuum ratio of the silicate features is too strong in comparison with the observed spectra for both stars. Moreover, the near-IR flux is often underestimated. This was also observed in Gielen et al. (2007), where we fitted the SED similarly to two post-AGB stars, RU Cen and AC Her. Including an extra continuum opacity source is needed to reduce the strength of the features (see Fig. 9) and to increase the near-IR contribution. From our previous work (Gielen et al. 2008) and Sect. 4.2, we found evidence that (a fraction of) the silicates might be iron poor. So we use metallic iron as a potential opacity source: its near-IR opacity is large, but the absorption coefficient is unfortunately featureless so direct detection is difficult. Inclusion of

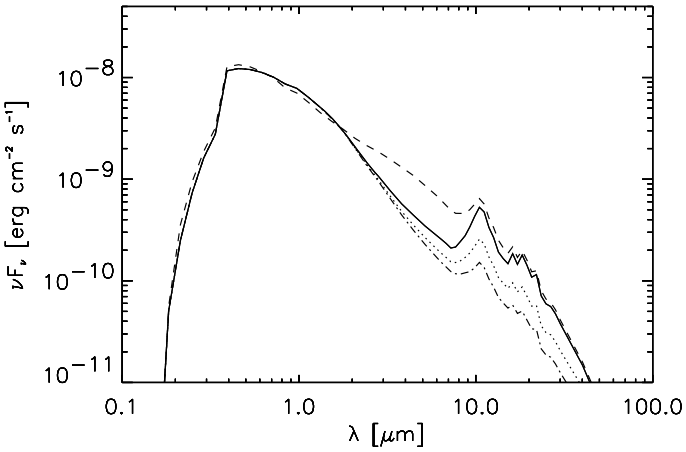

Fig. 9. Some SED disc models showing the influence of the inclusion of metallic iron and different grain sizes in the fitting. All models have the same physical parameters, the only difference being the amount of iron in the disc and the grain sizes. The solid line depicts a pure silicate disc with grain sizes between 0.1–20 μm. The dashed line represents a model with 5% metallic iron and 95% silicate with grain sizes between 0.1–20 μm. The dotted line represents a silicate disc model with grain sizes between 0.1–50 μm and the dot-dashed line one with grain sizes between 0.1–100 μm.

free metallic iron has a strong impact on the modelling because the near-IR excess increases significantly with a given inner radius. Another possible opacity source is the inclusion of hot large grains in the homogeneous disc model.

5.3.1. HD 52961

We can use the interferometric data for HD 52961 to constrain the distance to the system (Fig. 11). When we compare the modelled visibilities with the observations for HD 52961 we find that the visibilities of our model are too high, when using standard models of $L = 5000\,L_\odot$ which fit the SED and impose the inner radius to be at sublimation radius. This means we need to increase the angular size of the *N*-band emission region, either by increasing the physical size or by decreasing the distance. Increasing the disc size to outer radii >500 AU does not influence the *N*-band emission so we need to increase the inner radius, flatten the density distribution power law and/or decrease the luminosity in the disc model. Changing the surface-density distribution power law to values >-1.5 proved incompatible with the observed SED. We therefore use an average luminosity of $3000\,L_\odot$ and move the inner radius to larger distances. A good fit to the SED was obtained using an inner radius of 10 AU. This assumed luminosity gives a distance to the system of about 1700 pc. At 10 AU the temperature of the inner rim is around 1100 K, which is slightly below the canonical dust sublimation temperature for silicates.

For HD 52961 we tested models with and without the inclusion of metallic iron. The resulting fits can be seen in Fig. 10, parameters can be found in Table 5. Since this star shows a rather strong 10 μm feature, pointing to relatively large amounts of hot dust in the disc, we find we need a rather steep surface-density distribution, $\alpha < -1$. Since we only have one flux point at long wavelengths, we add a simple 160 K blackbody model to fit the observed submillimetre emission.

When no iron is included (model A) we see that the flux around from 2 to 8 μm is strongly underestimated. Including about 10% metallic iron (model B) increased this flux

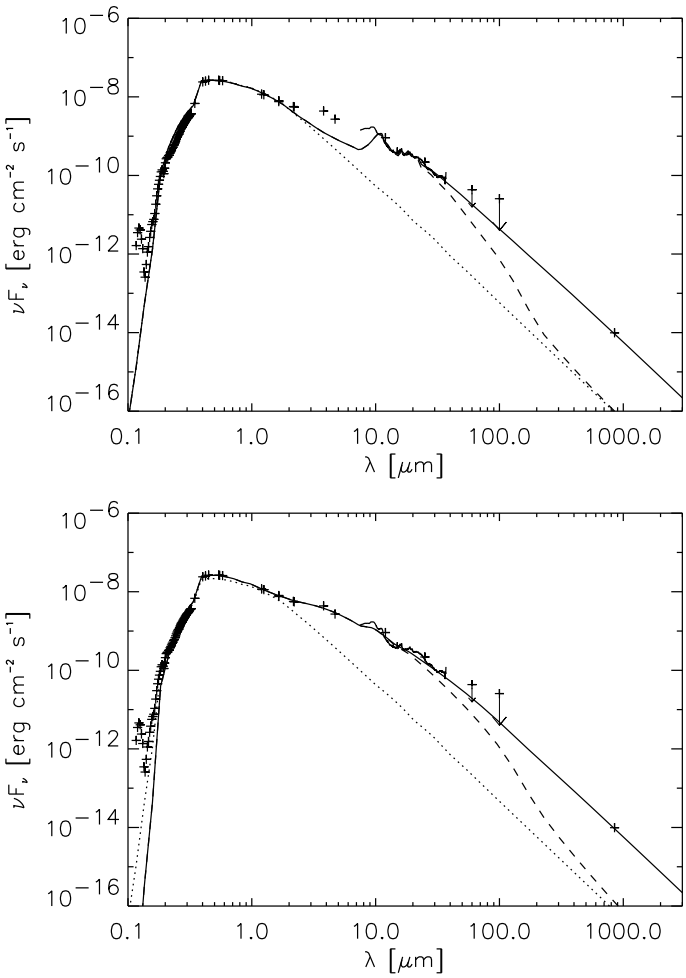

Fig. 10. SED disc modelling of HD 52961 (*top*: model A without metallic iron, *bottom*: model B with metallic iron). The dashed line represents the homogeneous disc model consisting of grains between 0.1 μm and 20 μm. The solid line gives the disc model with an added blackbody to represent the cool midplane. Crosses represent photometric data and in the infrared we overplot the observed Spitzer-IRS spectrum. The dotted line represents the adopted Kurucz stellar model.

Table 5. Results of our SED disc modelling.

	R_{in}–R_{out} AU	m $10^{-5}\,M_\odot$	α	iron %	T_{bb} K	i °
HD 52961: A	10–500	1.7	−1.5	0	160	0–90
HD 52961: B	10–500	0.7	−1.5	10	160	<65
EP Lyr: A	40–300	6	−1.0	0	–	0–90

Note: Given are the inner and outer radius (R_{in}–R_{out}), the total disc mass m for the homogeneous disc model, the surface-density distribution power law α, the percentage of iron in the homogeneous disc model, the blackbody temperature and the inclination of the system.

significantly. The inclusion of metallic iron has only a minor influence on the *N*-band interferometric measurements. It decreases the modelled visibilities by about 10%, which is still consistent with the observed visibilities.

The modelled visibilities (Fig. 11) lie within the observed visibility range but a remarkable detection is that the variation in visibilities between the two observations is quite large, despite the very limited difference in lengths (41.3–46.3 m), as well as in projected angle (45.6–46.3°). This is illustrated when we plot the visibility versus the spatial frequency for a given wavelength,

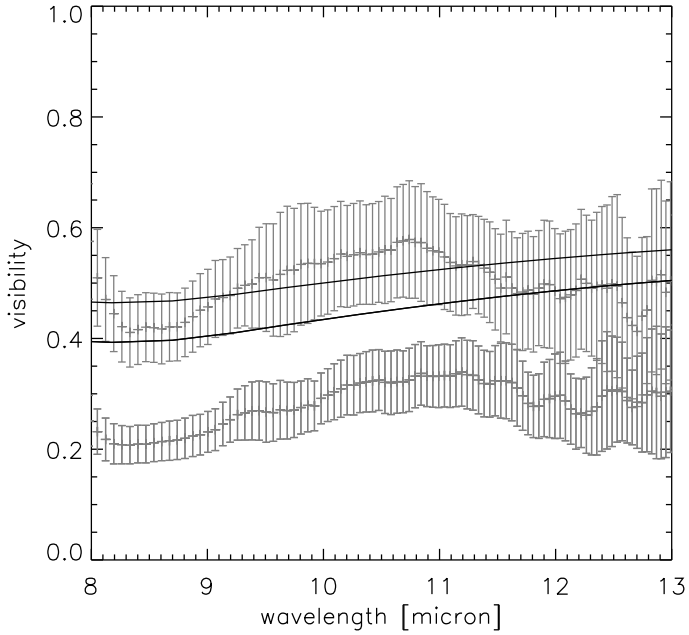

Fig. 11. The observed MIDI measurements of HD 52961 (gray data with error bars) and the visibilities deduced from disc model A (black solid line), for the two different baselines. The model has an inclination of 45° and a position angle on the sky of 227° East of North.

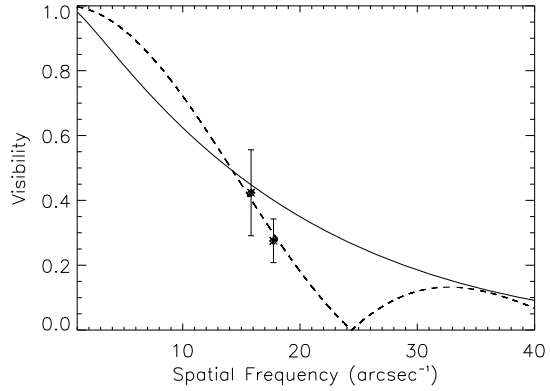

Fig. 12. Comparison between modelled and observed visibilities at 12.6 μm, at the two different baseline lengths. The dashed line represents a uniform disc model with an angular size of 50 mas. The solid line gives the visibilities as calculated from the 2D disc modelling (model B).

as seen in Fig. 12. In this figure we illustrate that when using a uniform disc for the intensity distribution, the steep visibility drop can be accounted for. The physical disc model is, however, much smoother and does not contain the very sharp edge characteristic of the uniform disc. The model also do not reproduce the observed "bump" in visibility between 9 and 12 μm. Deroo et al. (2006) explain this observed increase in visibility as being due to a non-homogeneous distribution of the silicates, which contribute most to the inner regions of the disc. The current disc model does not include the physics to be able to reproduce this radial distribution of dust species.

The submillimetre 850 μm flux for HD 52961 and the derived blackbody temperature of 160 K can be used to estimate the dust

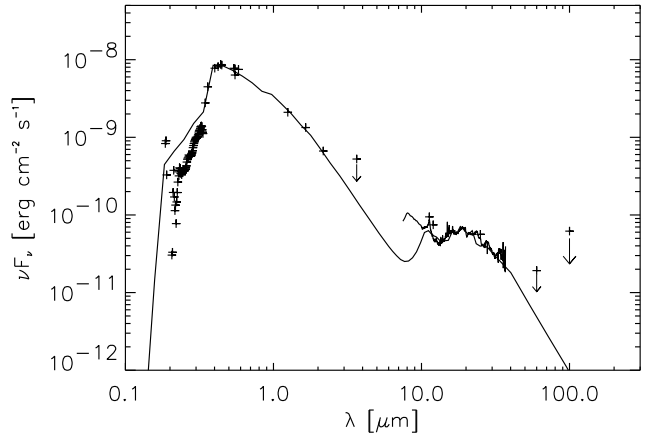

Fig. 13. The SED disc model of EP Lyr. The model parameters are given in Table 5.

mass of large grains in the disc. In the optically thin approach the disc mass can be estimated using (Hildebrand 1983)

$$M_{\rm d} = \frac{F_{850}\, D^2}{\kappa_{850}\, B_{850}(T)}.$$

Assuming a cross section of large spherical grains, the mass absorption coefficient of 850 μm grains in blackbody approximation is about 2.4 cm^2 g^{-1}. The mass absorption coefficient is given by $\kappa = \frac{\pi a^2}{\frac{4}{3}\pi a^3 \rho}$, with a the grain size, and ρ typically 3.3 g cm^{-3} for astronomical silicates. This results in dust-mass estimates in large grains of $3.2 \times 10^{-6}\, M_\odot$ for HD 52961.

5.3.2. EP Lyr

The SED-fitting gives an estimate of the distance to the system of $d = 3.4$ kpc, assuming a luminosity $L = 3000\, L_\odot$. This estimation is not only dependent on the assumed luminosity of the star, but also on the adopted inclination of the system. Other derived disc parameters can be found in Table 5.

For EP Lyr it proved very problematic to get a good fit to the observed strong 20 μm feature, without introducing a strong 10 μm silicate feature. The mixed chemistry adds to the complexity of the object as the PAH emission and underlying continuum in the near-IR may very well come from a distinct structural component, in for example the polar direction. This is already seen in HD 44179, were the observed PAH emission comes from a bipolar outflow (Bregman et al. 1993; Men'shchikov et al. 2002; Cohen et al. 2004). The lack of data shortwards of 7 μm makes it hard to get a good continuum estimate of the near- and mid-IR energetics. Cool dust clearly dominates the SED, but without additional information from interferometry, we cannot constrain parameters like the inner radius or the surface-density distribution. We opted to keep a rather flat density distribution of $\alpha = -1.0$ and do not force the model to fit the spectrum shortward of 15 μm.

To get a good fit to the SED a very large inner radius of about 40 AU is necessary. At this distance the inner rim reaches temperatures of ~300 K. This temperature agrees with the temperatures found in the spectral modelling (Sect. 4.2). If we include metallic iron in the model we find we need inner radii even larger than 200 AU, which seems physically implausible. Unfortunately we do not posses submillimetre data for this star

so we cannot determine the blackbody temperature associated with the midplane. The small L_{IR}/L_* as well as the lack of a near-IR dust excess shows that the inner rim is quite far from the sublimation radius.

6. Conclusions

HD 52961 and EP Lyr both have rich infrared spectra, and the assembled multi-wavelength data show that these evolved objects are surrounded by a stable circumstellar disc. While the binary nature of HD 52961 is well established, the binarity of EP Lyr is suspected but not yet firmly proven. The discs must be circumbinary as the sublimation radius of the dust is larger than the determined (HD 52961) and suspected (EP Lyr) binary orbit.

Recent studies have shown that many of these binary post-AGB systems are already detected (Van Winckel 2003; De Ruyter et al. 2006; Deroo et al. 2006, 2007a; Gielen et al. 2008), but EP Lyr and HD 52961 both show quite distinct characteristics in dust and gas chemistry as well as in physical properties of their discs.

EP Lyr and HD 52961 are the only stars from the larger Spitzer sample that have clear CO_2 gas emission lines in the mid-IR. Our modelling shows that the emission in both stars can be well fitted and is dominated by $^{12}C^{16}O_2$ features, but clear detections of other isotopes are present as well. Similar excitation temperatures and column densities are found in both objects, but with different ratios for $^{12}C^{16}O_2$ and $^{13}C^{16}O_2$. Why these two stars are the only ones from the larger sample showing strong CO_2 features, and if there is any relation with the low observed infrared flux remains unclear. Similar feature strengths observed in the other stars would have been easily detected. One possibility is that the low dust emission in the two sample stars, reflected in the low L_{IR}/L_{star}, makes it easier for the CO_2 gas to become visible. This effect is also seen in AGB stars, where CO_2 gas emission is strongest in sources with the lowest mass-loss rates (Sloan et al. 1996; Cami 2002; Sloan et al. 2003).

One of the most remarkable features is the clear detection of ^{18}O isotopes of CO_2 in both objects. Together with HR 4049 (Cami & Yamamura 2001), the strong $^{16}O^{12}C^{18}O$ band is a systematic feature of the gas emission in the discs of post-AGB binaries when CO_2 emission is detected. The high ^{18}O abundance of HR 4049 derived in an optically thin approximation of a putative nucleosynthetic origin (Lugaro et al. 2005) was not confirmed by the analysis of CO first overtone absorption (Hinkle et al. 2007) in the same object. It is likely that the CO_2 gas is strongly optically thick, also in EP Lyr and HD 52961, so that very rare isotopes are detectable.

The high-resolution Spitzer spectra also reveal unique solid state features. As in the bulk of the disc sources (Gielen et al. 2008), crystalline silicate features prevail in both stars, but unlike what we found for the larger sample, they proved very hard to model. In HD 52961 we observe some unique strong crystalline features at 11.3 and 16 μm, which could not be reproduced in the modelling, irrespective of the grain size used in the models, shape or assumed grain model. In the 2D disc modelling we could not fit the steep rise around 10 μm, without the inclusion of metallic iron. Combining our physical model constrained by the SED, together with our interferometric data, we concluded that the inner dust rim is slightly beyond the dust sublimation radius. This is in contrast to similar binary objects like IRAS 08544-4431 where the interferometric data shows that the dusty disc has to start very near to the dust sublimation radius (Deroo et al. 2007a). Assuming a luminosity of 3000 $L_\odot$, we find that the inner disc radius of HD 52961 is rather large, around 10 AU.

The strong 850 μm flux shows that this object has a component of very large grains. This contribution was added to the SED fitting by an additional colder Planck curve.

EP Lyr has only a very small infrared excess, but the Spitzer spectrum is very rich in spectral details. The most remarkable characteristic is the clear PAH emission, in combination with the strong crystalline features at longer wavelengths. There is no evidence that the central star evolved into a carbon star when on the AGB, yet unprocessed class-C PAH features are clearly detected. Whether these PAH species are formed in the circumbinary disc or in a recent, likely polar outflow of the depleted central star, remains unclear. An extra component of cold dust is necessary in this object as well, to fit the entire Spitzer spectrum. Unfortunately, EP Lyr is too faint for the current interferometric possibilities.

The mixed chemistry, the strongly processed cold crystalline silicates and low $^{12}C/^{13}C$ ratio are in common with the subgroup of silicate J-type carbon stars, which can also display strong crystalline material. This corroborates the conclusion that in the latter, the disc is circumbinary. The abundance studies of J-type carbon stars are not complete enough to probe whether photospheric depletion affected these objects as well.

Both objects are extreme examples of post-AGB binary stars, with characteristics dominated by the presence of a stable circumbinary disc. This disc environment is, to first order, well modelled by assuming a passive, irradiated stable disc. In this paper we corroborate that this geometry is ideal to induce strong grain processing and a rich, even mixed chemistry. We conclude also that a homogeneous disc model is too primitive to model the spectral details as evidence of grain settling is strong. The route to PAH formation (and excitation) in the O-rich EP Lyr remains to be studied in detail as PAH emission is only observed in a very limited number of such sources.

This detailed study of HD 52961 and EP Lyr shows that many questions still remain in our current understanding of the evolution of a significant number of post-AGB binary stars, and the impact of the circumbinary discs on the entire system.

Acknowledgements. C.G. acknowledges support of the Fund for Scientific Research of Flanders (FWO) under the grant G.0178.02. and G.0470.07.

References

Abia, C., & Isern, J. 2000, ApJ, 536, 438
Antoniucci, S., Paresce, F., & Wittkowski, M. 2005, A&A, 429, L1
Bregman, J. D., Rank, D., Temi, P., Hudgins, D., & Kay, L. 1993, ApJ, 411, 794
Bujarrabal, V., Castro-Carrizo, A., Alcolea, J., & Neri, R. 2005, A&A, 441, 1031
Cami, J. 2002, Ph.D. Thesis, University of Amsterdam
Cami, J., & Yamamura, I. 2001, A&A, 367, L1
Cohen, M., Anderson, C. M., Cowley, A., et al. 1975, ApJ, 196, 179
Cohen, M., Barlow, M. J., Sylvester, R. J., et al. 1999, ApJ, 513, L135
Cohen, M., Van Winckel, H., Bond, H. E., & Gull, T. R. 2004, AJ, 127, 2362
De Ruyter, S., Van Winckel, H., Dominik, C., Waters, L. B. F. M., & Dejonghe, H. 2005, A&A, 435, 161
De Ruyter, S., Van Winckel, H., Maas, T., et al. 2006, A&A, 448, 641
Deroo, P., Van Winckel, H., Min, M., et al. 2006, A&A, 450, 181
Deroo, P., Acke, B., Verhoelst, T., et al. 2007a, A&A, 474, L45
Deroo, P., Van Winckel, H., Verhoelst, T., et al. 2007b, A&A, 467, 1093
Dominik, C., Dullemond, C. P., Cami, J., & van Winckel, H. 2003, A&A, 397, 595
Dullemond, C. P., & Dominik, C. 2004, A&A, 417, 159
Dullemond, C. P., Dominik, C., & Natta, A. 2001, ApJ, 560, 957
Furlan, E., Hartmann, L., Calvet, N., et al. 2006, ApJS, 165, 568
García-Hernández, D. A., Abia, C., Manchado, A., & García-Lario, P. 2006, A&A, 452, 1049
Gielen, C., Van Winckel, H., Waters, L. B. F. M., Min, M., & Dominik, C. 2007, A&A, 475, 629
Gielen, C., Van Winckel, H., Min, M., Waters, L. B. F. M., & Lloyd Evans, T. 2008, A&A, 490, 725

Giridhar, S., Lambert, D. L., & Gonzalez, G. 2000, ApJ, 531, 521
Gonzalez, G., Lambert, D. L., & Giridhar, S. 1997, ApJ, 479, 427
Gutenkunst, S., Bernard-Salas, J., Pottasch, S. R., Sloan, G. C., & Houck, J. R. 2008, ApJ, 680, 1206
Hildebrand, R. H. 1983, QJRAS, 24, 267
Hinkle, K. H., Brittain, S. D., & Lambert, D. L. 2007, ApJ, 664, 501
Hony, S., Van Kerckhoven, C., Peeters, E., et al. 2001, A&A, 370, 1030
Hony, S., Waters, L. B. F. M., & Tielens, A. G. G. M. 2002, A&A, 390, 533
Hony, S., Tielens, A. G. G. M., Waters, L. B. F. M., & de Koter, A. 2003, A&A, 402, 211
Houck, J. R., Roellig, T. L., van Cleve, J., et al. 2004, ApJS, 154, 18
Izumiura, H., Noguchi, K., Aoki, W., et al. 2008, ApJ, 682, 499
Johnson, J. J., Anderson, C. M., Bjorkman, K. S., et al. 1999, MNRAS, 306, 531
Jura, M. 1986, ApJ, 309, 732
Jura, M. 2003, ApJ, 582, 1032
Jura, M., & Kahane, C. 1999, ApJ, 521, 302
Jura, M., Bohac, C. J., Sargent, B., et al. 2006, ApJ, 637, L45
Justtanont, K., Feuchtgruber, H., de Jong, T., et al. 1998, A&A, 330, L17
Kemper, F., Molster, F. J., Jäger, C., & Waters, L. B. F. M. 2002, A&A, 394, 679
Kessler-Silacci, J., Augereau, J.-C., Dullemond, C. P., et al. 2006, ApJ, 639, 275
Kholopov, P. N., Samus, N. N., Frolov, M. S., et al. 1999, VizieR Online Data Catalog, 2214, 0
Kraemer, K. E., Sloan, G. C., Bernard-Salas, J., et al. 2006, ApJ, 652, L25
Kwok, S., Volk, K. M., & Hrivnak, B. J. 1989, ApJ, 345, L51
Lahuis, et al. 2006, c2d Spectroscopy Explanatory Supplement, Cores to Disks, Spitzer Legacy Team, (Pasadena: Spitzer Science Center)
Lattanzio, J., Frost, C., Cannon, R., & Wood, P. R. 1996, Mem. Soc. Astron. Ital., 67, 729
Little-Marenin, I. R. 1986, ApJ, 307, L15
Lloyd Evans, T. 1990, MNRAS, 243, 336
Lloyd Evans, T. 1991, MNRAS, 249, 409
Lugaro, M., Pols, O., Karakas, A. I., & Tout, C. A. 2005, Nucl. Phys. A, 758, 725
Mastrodemos, N., & Morris, M. 1999, ApJ, 523, 357
Matsuura, M., Yamamura, I., Cami, J., Onaka, T., & Murakami, H. 2002, A&A, 383, 972
McSaveney, J. A., Wood, P. R., Scholz, M., Lattanzio, J. C., & Hinkle, K. H. 2007, MNRAS, 378, 1089
Men'shchikov, A. B., Schertl, D., Tuthill, P. G., Weigelt, G., & Yungelson, L. R. 2002, A&A, 393, 867
Menut, J.-L., Chesneau, O., Bakker, E., et al. 2009, A&A, 496, 133
Miyake, K., & Nakagawa, Y. 1995, ApJ, 441, 361
Molster, F. J., Yamamura, I., Waters, L. B. F., et al. 2001, A&A, 366, 923
Molster, F. J., Waters, L. B. F. M., & Tielens, A. G. G. M. 2002, A&A, 382, 222
Ohnaka, K., & Tsuji, T. 1999, A&A, 345, 233
Ohnaka, K., Izumiura, H., Leinert, C., et al. 2008, A&A, 490, 173
Peeters, E., Hony, S., Van Kerckhoven, C., et al. 2002, A&A, 390, 1089
Peeters, E., Mattioda, A. L., Hudgins, D. M., & Allamandola, L. J. 2004, ApJ, 617, L65
Preston, G. W., Krzeminski, W., Smak, J., & Williams, J. A. 1963, ApJ, 137, 401
Reyniers, M., Van Winckel, H., Gallino, R., & Straniero, O. 2004, A&A, 417, 269
Reyniers, M., Abia, C., van Winckel, H., et al. 2007, A&A, 461, 641
Rothman, L. S., Jacquemart, D., Barbe, A., et al. 2005, J. Quant. Spectrosc. Radiat. Transf., 96, 139
Ryde, N., Eriksson, K., & Gustafsson, B. 1999, A&A, 341, 579
Schneller, H. 1931, Astron. Nachr., 243, 99
Sloan, G. C., Levan, P. D., & Little-Marenin, I. R. 1996, ApJ, 463, 310
Sloan, G. C., Kraemer, K. E., Goebel, J. H., & Price, S. D. 2003, ApJ, 594, 483
Sloan, G. C., Keller, L. D., Forrest, W. J., et al. 2005, ApJ, 632, 956
Sloan, G. C., Jura, M., Duley, W. W., et al. 2007, ApJ, 664, 1144
Sloan, G. C., Kraemer, K. E., Wood, P. R., et al. 2008, ApJ, 686, 1056
Sylvester, R. J., Skinner, C. J., & Barlow, M. J. 1998, MNRAS, 301, 1083
Tielens, A. G. G. M. 2008, ARA&A, 46, 289
Van Winckel, H. 2003, ARA&A, 41, 391
Van Winckel, H. 2007, Baltic Astron., 16, 112
Van Winckel, H., & Reyniers, M. 2000, A&A, 354, 135
Van Winckel, H., Mathis, J. S., & Waelkens, C. 1992, Nature, 356, 500
Van Winckel, H., Waelkens, C., & Waters, L. B. F. M. 1995, A&A, 293, L25
Van Winckel, H., Waelkens, C., Waters, L. B. F. M., et al. 1998, A&A, 336, L17
Van Winckel, H., Waelkens, C., Fernie, J. D., & Waters, L. B. F. M. 1999, A&A, 343, 202
Volk, K., Kwok, S., & Hrivnak, B. J. 1999, ApJ, 516, L99
Waelkens, C., Lamers, H. J. G. L. M., Waters, L. B. F. M., et al. 1991a, A&A, 242, 433
Waelkens, C., Van Winckel, H., Bogaert, E., & Trams, N. R. 1991b, A&A, 251, 495
Waters, L. B. F. M., Trams, N. R., & Waelkens, C. 1992, A&A, 262, L37
Waters, L. B. F. M., Molster, F. J., de Jong, T., et al. 1996, A&A, 315, L361
Waters, L. B. F. M., Cami, J., de Jong, T., et al. 1998, Nature, 391, 868
Werner, M. W., Roellig, T. L., Low, F. J., et al. 2004, ApJS, 154, 1
Willacy, K. 2004, ApJ, 600, L87
Witt, A. N., Vijh, U. P., Hobbs, L. M., et al. 2008, ArXiv e-prints
Yamamura, I., Dominik, C., de Jong, T., Waters, L. B. F. M., & Molster, F. J. 2000, A&A, 363, 629
Zsoldos, E. 1995, A&A, 296, 122